Synthesis, characterization, and biological activity of oxidovanadium(IV) hydroxamate complexes supported by density functional theory

Sonika Sharma[a], Debasish Das[b,*], Biswajit Sadhu[c], Neeraj Sharma[a]

[a]Department of Chemistry, Himachal Pradesh University, Summer Hill, Shimla-171005, India

[b]Waste Management Division, Bhabha Atomic Research Centre, Trombay, Mumbai-400085, India

[c]Health Physics Division, Bhabha Atomic Research Centre, Trombay, Mumbai-400085, India

*Corresponding author email: deba.chem@gmail.com, debads@barc.gov.in

Abstract

The oxidovanadium(IV) complex $[VO(HL)_2]$ (**1**) (where, HL = 4-nitrocinnamohydroxamate; 4-$NO_2C_6H_4CH=CHCONHOH$) has been synthesized by the condensation reaction of $VOSO_4{\cdot}5H_2O$ and potassium 4-nitrocinnamohydroxamate in methanol-water medium. The complex is characterized by elemental analysis, molar conductivity, magnetic susceptibility measurement, FTIR, UV-Vis, Electron Paramagnetic Resonance (EPR) spectral techniques and mass spectrometry. The bidentate linkage of hydroxamate ligand involving O,O-coordination through hydroxamic and carbonyl oxygen atoms has been deduced. The magnetic susceptibility, EPR and mass spectra (ESI-MS) indicate that the complex exists as monomer and a distorted square pyramidal geometry around vanadium is proposed. The electrochemical study of **1** has shown it is to be electrochemically active exhibiting VO^{V}/VO^{IV} quasi-reversible redox couple. The thermal study of the complex yielded VO_2 as sole decomposition product. The coordination compounds **2** and **3** have been isolated from the reaction of complex **1** with 2-cyanopyridine (2-CNPy) and 4-aminobenzonitrile (4-CNAn) respectively and characterized by physicochemical and IR spectral study. The biological activity of **1**-**3** has been studied against various pathogenic bacteria *E. coli, S. aureus, S. typhi, S. paratyphi, S. epidermidis, K. pneumonia* and fungi *C. albicans, B. fulva,* and *F. oxysporum* by minimum inhibitory concentration (MIC) method. The complexes exhibit enhanced antimicrobial activity relative to both the free ligand and vanadyl sulphate. The cytotoxicity of **1-3** has been studied on mammalian transformed cell line Hep2c, a derivative of human cervix carcinoma HeLa cells by MTT assay. **2** and **3** exhibit higher cytotoxic activity than **1** and reveal a marked effect of the coordination of nitrogen bases. Density functional theory studies have been carried out to determine the relative free energy of

formation and stable molecular structures of **1-3**. Time dependent density functional theory (TD-DFT) based calculation have been performed to find out the frontier molecular orbitals and to corroborate with the experimentally observed UV-Vis spectrum of **1**. Other parameters like HOMO, and LUMO energies, density of state (DOS), and global reactivity descriptors clearly support higher biological activity of **2** and **3** than **1**.

Keywords: Vanadium complex, Nitrogen bases, Spectral studies, Antimicrobial activity, Cytotoxicity

1. Introduction

Research in chemical sciences has flourished with many advances in last few decades of which vanadium compounds present very interesting and enriched chemistry towards biochemical and pharmacological properties [1-4]. Vanadium is an essential nutrient element, but unfortunately have some toxic effects [5,6]. Complexation by organic ligands is one of the effective ways to improve the vanadium efficacy and decrease the toxic side effects. The potential applications of vanadium complexes as molecular magnets and in material science are well documented [7-16]. Moreover, the significant role of vanadium complexes in biological nitrogen fixation, haloperoxidation, catecholase [17,18] and antimicrobial activity [19] has drawn a particular attention. The coordinated form of vanadium as oxovanadium(IV) and (V) ions i.e., VO^{2+}, VO^{3+}, VO_2^+ and $VO(O_2)^+$ has gathered tremendous research interest. The vanadyl ion is believed to be enriched in seaweeds and blood stream of the higher animal species [20]. Vanadyl complexes composed of pyrazole based N-donor ligands have displayed very interesting biochemical and pharmacological properties such as insulin-mimetic properties [21], as well as antiparasitic [22,23] and antitumor ones [24-26].

Among the biologically important ligands, hydroxamic acids having RCONHOH group, the derivative of both hydroxylamine and carboxylic acids [27-29] constitute an important class of organic bioligands, due to their broad spectrum of biological and pharmacological activities. Hydroxamate based ligands also possess potential applications as reagents in analytical chemistry and have attracted overwhelming interest of inorganic chemists [30]. A perusal of literature revealed that of many known transition metal hydroxamate complexes [31], there are sporadic reports on vanadium-hydroxamate complexes [32-33]. The ligand potassium 4-nitrocinnamohydroxamate has been selected owing to the biological and pharmacological

(antioxidant, anxiolytic, insect repellent, antidiabetic, anticholesterolemic), fluorescent properties shown by cinnamic acid derivatives [34-37]. Thus, in continuation of our research interest in vanadium chemistry [38-48], a vanadium complex [$VO(4\text{-}NO_2C_6H_4CH{=}CHCONHO)_2$], **1** has been synthesized and thoroughly characterized by spectroscopic techniques. The coordination compounds of **1** with 4-aminobenzonitrile and 2-cyanopyridine have also been prepared and characterized. The antimicrobial potential of complexes **1-3** has been evaluated against pathogenic bacteria and fungi and exhibits encouraging results. The density functional theory calculations have been made to determine molecular structures and various reactivity descriptors of the synthesized complexes. TD-DFT calculation supports the observed electronic transitions of complex **1** quite satisfactorily.

2. Experimental

2.1 Materials and Methods

All chemicals used were of analytical grade and were purchased from Merck, India. The potassium 4-nitrocinnamohydroxamate was synthesized by reported method [49]. The vanadium content in complexes was determined gravimetrically as V_2O_5 and C, H and N analyses were obtained on a Carlo-Erba 1108 elemental analyzer. The molar conductance measurements were performed on Elico Conductivity Bridge type CM-82T. FTIR spectra of complexes were recorded on a Nicolet-5700 FTIR spectrophotometer (4000-200 cm^{-1}) using KBr pellets. The room temperature magnetic susceptibility of **1** was measured by Gouy's method using $Hg[Co(NCS)_4]$ as calibrant. UV-Vis spectrum of **1** was recorded on a Varian Cary100 Bio UV-Vis spectrophotometer using methanol. The mass spectra were recorded at room temperature as electron spray ionization mass spectrometry (ESI-MS). The electrochemical study was carried out on CH instrument electrochemical analyzer. The cyclic voltammetric experiment was performed in single compartmental cell of volume 10-15mL containing a three–electrode system comprising of Pt-disk working electrode, Pt-wire as auxiliary electrode and an Ag/AgCl electrode as reference electrode in MeOH + H_2O (95:5) medium with Bu_4NClO_4 as supporting electrolyte. Thermogram of complexes was recorded on EXSTAR TG/DTA 6300 at a heating rate of $10^oC\ min^{-1}$ under nitrogen atmosphere.

2.2 Syntheses

2.2.1 Synthesis of $[VO(HL)_2]$ (1)

To a solution of $VOSO_4 \cdot 5H_2O$ (0.5 g, 1.95 mmol) in 20 mL of methanol:water (4:1 v/v), a solution of potassium-4-nitrocinnamohydroxamate, KHL (0.95g, 3.86 mmol) dissolved in methanol (20 mL) was added. The resultant solution was stirred for 1 h at room temperature. The solution was filtered and the filtrate was concentrated under vacuum by repeatedly treating with petroleum ether whereupon a dark brown solid product, **(Scheme 1)** soluble in DMSO and methanol, was obtained. The stoichiometric composition of **1** is consistent with the formula $VO(4\text{-}NO_2C_6H_4CH{=}CHCONHO)_2$. The cryoscopic molecular weight determination of **1** in nitrobenzene indicated that it exists as monomer in this solvent. It was recrystallized from dichloromethane. Yield: 0.80 g, 85%, Anal. Calcd. for $VC_{18}H_{14}O_9N_4$ (M.W: 480.94) (%) C, 44.92; H, 2.93; N, 11.64; V, 10.60. Found (%) C, 44.98; H, 2.98; N, 11.68; V, 10.65. Λ_m ($PhNO_2$): 1.06Sm^2mol^{-1}; μ_{eff} (293K): 1.71 B.M (Table S1).

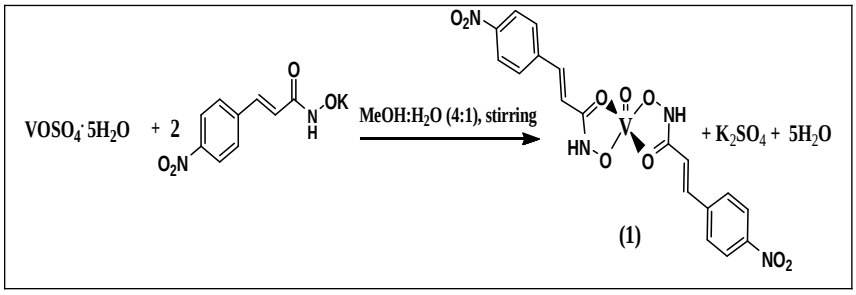

Scheme 1

2.2.2 Synthesis of $[VO(HL)_2(2\text{-}CNpy)]$ (2)

To a methanolic solution of $[VO(HL)_2]$ (0.57 g, 1.2 mmol), an equimolar amount of 2-cyanopyridine (2-CNpy) (0.125g, 1.2 mmol) was added. The solution was then stirred for 4 h at room temperature during which the formation of dark brown precipitates was observed **(Scheme 2)**. The precipitate was filtered, washed with petroleum ether and dried under vacuum. Yield: (0.55g, 80%); Anal. Calcd. For $VC_{24}H_{18}O_9N_6$ (M.W: 585.38) (%): C, 49.23; H, 3.10; N, 14.36; V, 8.72. Found: C, 49.19; H, 3.19; N, 14.40; V, 8.79, Λ_m = 3.58 Sm^2mol^{-1}; μ_{eff} = 1.74 B.M (Table S1).

2.2.3 Synthesis of $[VO(HL)_2(4\text{-}CNAn)]$ (3)

To a methanolic solution of $[VO(HL)_2]$ (0.50 g, 1.05 mmol), an equimolar amount (0.125 g, 1.05 mmol) of 4-aminobenzonitrile (4-CNAn) was added. The solution was then allowed to stir for 3 h at room temperature. The dark brown precipitate was formed, filtered and washed with petroleum ether **(Scheme 2)**. It was dried under vacuum. Yield (0.49 g, 79%); Anal. Calcd. For $VC_{25}H_{20}O_9N_6$ (M.W: 599.40) (%): C, 50.09; H, 3.36; N, 14.07; V, 8.54. Found: C, 50.01; H, 3.41; N, 14.09; V, 8.59; Λ_m = 5.60 Sm^2mol^{-1}; μ_{eff} = 1.72 B.M (Table S1).

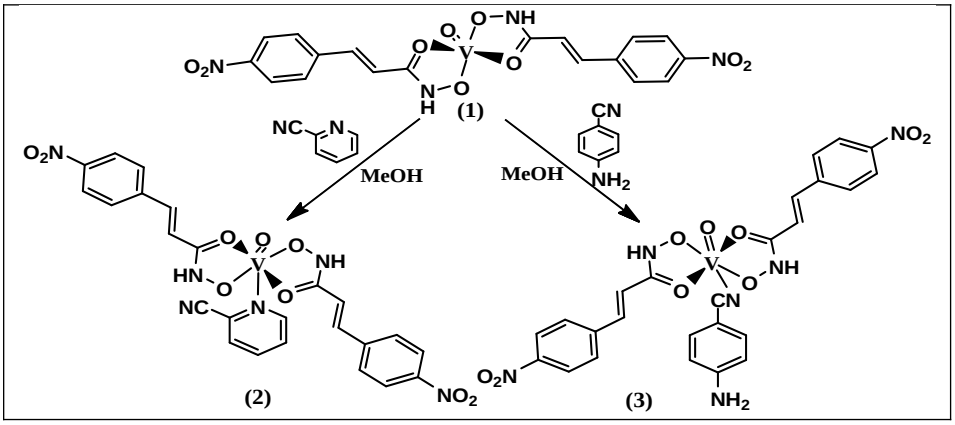

Scheme 2

2.3 Antimicrobial activity test

The hydroxamate ligand, vanadyl sulphate and complexes **1-3** were tested *in vitro* for their antimicrobial activity against some *Gram (+ve)* and *Gram (-ve)* bacterial species and pathogenic fungi by minimum inhibitory concentration (MIC) method [50-51] different concentrations (1 mg mL^{-1}) in DMSO recommended by National Committee for Clinical Laboratory Standard (NCCLS). All the samples were tested in triplicate and average values are considered. All test cultures were streaked on soya bean casein agar (SCDA) and incubated overnight at 37°C. The MIC assay was performed in a 96-well microtitreplate. For MIC assay of each test complex, a 12 row wells was used out of which last two wells were taken as control. Each of the ten wells received 100µL of the Mueller-Hinton broth except the first well that received 200 µL of broth containing 500 µg mL^{-1} concentration of the test drug. From the first well (containing test drug), 100 µL broth was taken out with a sterile tip and added to the broth in the second well and the contents were mixed several times. Then 100 µL was taken out from the second well and was added to the third well. In this way a range of two-fold serial dilutions were prepared (500-0.98 µg mL^{-1}) in DMSO. The broth in each well was inoculated with 2µL of the bacterial culture and 5 µL of fungal culture and the contents were mixed by 10 clockwise and 10 anticlockwise rotations on flat surface. The plate was incubated at 35°C and 30°C for bacteria and fungi

respectively. Their growth was monitored after 24 h and 5 days for fungi and bacteria respectively. The results were repeated five times and standard deviation was recorded. The results were compared with standard antifungal and antibacterial drugs viz. fluconazole (treated control) and tetracycline hydrochloride (TCH) respectively.

2.4 Cell culture

Human Cervix carcinoma (HeLa derivative cells) Hep2C (Catalogue number 85020207) susceptible to arboviruses and measles virus was used. The line carries several HeLa marker chromosomes indistinguishable from HeLa by STR HeLa, Ethnicity: Black. The cells were trypsinized from a confluent monolayer culture obtained in a 25 cm^2 canted neck flask. The confluent monolayer of the cells was washed two times with phosphate-buffer saline (pH 7.2) followed by exposure to Trypsin-EDTA (100 mg % EDTA and 125 mg % Trypsin 1:250; Sigma Chemical Co. St. Louis, USA) disaggregating solution for two minutes. The disaggregating solution was then removed and the treated flask was incubated at 37^oC for 3-5 minutes. The disaggregated cells were resuspended in appropriate volume of Eagels's medium (DMEM) supplemented with fetal calf serum (10%, v/v) and adjusted to a cell density of 4×10^3 cells/mL which were then used for testing the complexes.

2.5 *In Vitro* cytotoxicity assay

The uniform mixture of Hep2C cell suspension (200 µL/well) was poured in the selected tissue culture plate with 96-wells. The drug compounds prepared in DMSO (0.1 M stock) in wells under each of the columns, was dispensed to achieve final concentration of 2, 4, 8, 20 and 28mM. The cells which are treated with drug compound were incubated in a CO_2 incubator at 37^oC for 16-18 h. The concentration of each of the drug compounds were tested four times and average values were calculated after MTT assay (using 5mgmL^{-1} in PBS, 0.1 M pH 7.2 of MTT (1-(4,5-dimethylthiazol-2-yl)-3,5-diphenylformazan). The appropriate controls with no drug added which contain appropriate amount of DMSO (medium for preparing stock of drug compounds) were also incubated to observe the effect of DMSO alone on the possibility of the proliferating cells cultured in vitro.

2.6 Theoretical study

In the present study, TURBOMOLE-7.0 software is used for all the DFT related calculations [52]. For time dependent density functional theory (TD-DFT) calculations, ADF 2017 [53] package is utilized. The geometry of 4-nitrocinnamohydroxamate ligand, $VOSO_4{\cdot}5H_2O$ as well

as their complexes **1**-**3** have been optimized in gas phase using Becke exchange and Perdew correlation (BP86) GGA (Generalized Gradient Approximation) functional and def2-TZVP basis set for all the atoms. This method is represented as BP86/DEF throughout the paper. For vanadium, spin-unrestricted open shell configuration (doublet state) is considered for V^{4+} ($3d^1$) ion. Tight energy convergence (10^{-8}eV between two consecutive self-consistent field (SCF) steps) and one-electron density matrix ($denconv $1d^{-7}$) convergence criteria with grid size 4 is applied for high accuracy of the calculations. RI-DFT based calculations were performed to speed up the calculations which employ the Resolution of the Identity approach for computing the electronic Coulomb interaction (RI-J). The local minima in potential energy surface are confirmed by computing the vibrational frequencies which are found to be with all real values. Single point energy calculations in methanol-water (4:1 v/v) mixed solvent (ε = 41.0) and CH_3OH (ε = 33.0) have been carried out to implement solvent effect using conductor like screening model (COSMO) [54]. The binding energy of the complexes has been calculated in gas phase and in solvent phase using free energy corrections at 298.15 K for the latter. Furthermore, the charge distribution study has been performed using natural population analysis (NPA) and Mulliken population analysis method. Density of states (DOS), partial density of states (PDOS) and overlap population density-of-states (OPDOS) calculations have been executed using MultiWFN software [55]. The binding energies of **1**(cis and trans), and complexes **2** and **3** have been calculated using the following equations:

$$VOSO_4{\cdot}5H_2O + 2HL^- = VO(HL)_2 + SO_4^{2-} + 5H_2O;$$

$$BE = E[VO(HL)_2] + E[SO_4^{2-}] + 5*E[H_2O] - E[VOSO_4{\cdot}5H_2O] - 2*E[HL^-]$$

$$VO(HL)_2 + B = VO(HL)_2{\cdot}B;$$

$$BE = E[VO(HL)_2{\cdot}B] - E[VO(HL)_2] - E[B]$$

where, HL = 4-nitrocinnamohydroxamate, and B = 2-CNpy or 4-CNAn.

3. Results and discussion

3.1 Vibrational Spectroscopy

The formation of **1** has been inferred from a comparison of its FTIR spectrum with that of metal precursor (Figure S1) and uncoordinated hydroxamate ligand (Figure S2) in 4000-400 cm^{-1} region. The characteristic bands of υ(C–N), υ(C=O), υ(N–H), and υ(N–O) vibrations in hydroxamate ligand is expected to undergo significant change on complexation with metal ions. The free potassium-4-nitrocinnamohydroxamate exhibited bands at 3108, 1637, 1341 and 920

cm^{-1} due to υ(N–H), υ(C=O), υ(C–N), and υ(N-O) vibrational modes respectively. In complex **1**, these bands are found to appear at 3101, 1518, 1392, and 926cm^{-1} respectively (Figure S3). A significant shift in υ(C=O) vibration to lower and υ(C-N) vibration to higher wave number may be ascribed to electron transfer  from the carbonyl oxygen to the vanadium atom with simultaneous strengthening of the C-N bond through resonance and also suggestive the coordination through the carbonyl oxygen. A shift in υ(N-O) mode to lower frequency is indicative of simultaneous bonding through hydroxyl amine oxygen atoms [56-57]. The υ(N–H) mode remained almost unshifted. The absorption band observed at 1045 cm^{-1} has been assigned to υ(V=O) mode. Appearance of new band at 484 cm^{-1} may be assigned to υ(M-O) bond [58]. The υ(O-H) band that appeared at 2831 cm^{-1} in free hydroxamate get disappeared in complex, indicative of deprotonation of -OH group.

3.2 Electronic absorption spectra

The UV/Vis spectrum of $VOSO_4 \cdot 5H_2O$ is found to exhibit bands at 252, 306 and 780 nm in consonance with most of the reported vanadyl complexes [59]. The UV-Vis spectrum of complex **1** was recorded in methanol solvent. The free potassium 4-nitrocinnamohydroxamate (KHL) displayed absorption bands at 246 (ϵ = 2890 $Lmol^{-1}cm^{-1}$), 258 (2410 $Lmol^{-1}cm^{-1}$), and 290 (2990 $Lmol^{-1}cm^{-1}$) nm which are attributed to intraligand $\pi \rightarrow \pi^*$ transitions. **1** showed four absorption bands at 386 (1175 $Lmol^{-1}cm^{-1}$), 422 (678 $Lmol^{-1}cm^{-1}$), 580 (140 $Lmol^{-1}cm^{-1}$), and 710 (42 $Lmol^{-1}cm^{-1}$) nm which may be designated to metal induced charge transfer transition. The less intense absorption band appeared at 580 nm may be ascribed to ^2Eg-$^2T_{2g}$ transition characteristic of oxidovanadium(IV) coordinated by strong π donating ligands. The absorption band at 422 nm may be due to the LMCT transition originating from lone pair of electrons on oxygen atom of hydroxamate ligand into an empty d-orbital of the vanadium ion [60]. The absorption band observed at 710 nm may be stipulated to be originated from a lone pair of O p-orbitals on the hydroxamate ligand into an empty d-orbital of vanadium to produce strong ligand to metal ($L \rightarrow M$) charge transfer (LMCT).

3.3 ESR spectroscopy

The X-band ESR spectrum of complex **1** at room-temperature displayed a well-resolved eight lines spectrum typically seen in vanadium(IV) complexes due to the interaction of an unpaired electron with its own nucleus, nuclear spin quantum number (I = 7/2) consistent with a single paramagnetic vanadium(IV). The g-average values obtained from the spectrum is ~1.98, which is

very closer to the spin only value of 2.00 and suggesting negligible contribution of spin-orbit coupling (Table S2).

3.4 Mass Spectrometry

The mass spectrum of complex **1** (Figure S4) displayed molecular ion peak and other related smaller fragment ions, confirmed its composition (Table S3). The oxidovanadium(IV) complex **1** displayed peaks at m/z 479 (37.65) and 478 (100) corresponding to $[M-2H]^+$ and $[M-3H]^+$ species respectively. The other structurally important intense fragment ions appeared at m/z 371 (7.7), 274 (13.99), 210 (7.78), 189 (8.25), 149 (6.52), 102 (4.87) which could be assigned to $[VO(HL)_2 2NO_2\text{-}O\text{-}2H]^+$, $[VO(HL)]^+$, $[HL+3H]^+$, $[VO(CONHO)_2+4H]^+$, $[HL\text{-}CONHO+2H]^+$ and $[HL\text{-}CONHO\text{-}NO_2+H]^+$ respectively.

3.5 Electrochemical studies

Electrochemical studies can provide useful information about redox processes, heterogeneous electron transfer reaction kinetics and chemical reactions consists of redox couple. Vanadium has many stable oxidation states therefore exhibiting redox activity is very common in vanadium complexes where the bonded ligands (innocent) do not play any role. In order to studythe ligand binding and its effects on redox properties, the electrochemical study of oxidovanadium(IV) complex by cyclic voltammetry have been performed (Figure S5). A negative scan was navigated towards positive direction in the potential range -2.0 to +2.0 which resulted one peak at +1.0 due to the oxidation of the ligand HL (Table S4). Complex of composition **1** displayed a single anodic and a cathodic peak. Peak-to-peak separation for the cathodic and anodic waves of 60-70 mV is indicative of one electron quasi-reversible metal-centered reduction. The electrode processcan therefore be represented as:

$$[VO^{IV}(HL)_2] \rightleftharpoons [VO^{V}(HL)_2] + e^{-1}$$

The increased stability of complex is known to shift the electrochemical reduction of central ion towards the more negative potential.

3.6 Thermal Studies

The thermal decomposition behavior of $[VO(HL)_2]$ (**1)** was studied via TG and DTA techniques under N_2 atmosphere (Figure S6). The TG curve of **1** has indicated that it is thermally stable up to 200^{o}C after which temperature it undergoes decomposition in a single step. The mass loss of 83.05 % in 200-333^{o}C range is indicative to yield VO_2 as the decomposition product. Similar type of formation of VO_2 as the product of decomposition is in agreement with thermal

decomposition of vanadium(IV) hydroxamates and vanadium(IV) formate complexes [61]. The IR spectrum of the residue hasshown sharp absorption band at 998 cm^{-1} due to υ(V=O) mode and other bands appeared at 672, 660, 625, 525, and 320 $cm^{-1}$are in conformity with other reports [62]. DTG curve exhibited a broad doublet at 275 and 313ºC and DTA curve displayed a feeble exothermic peak at 326ºC.

3.7 Magnetic studies

The magnetic susceptibility measurement of the finely powdered oxovanadium(IV) hydroxamate complexes **1**,**2**, and **3** was measured at room temperature using $Hg[Co(NCS)_4]$ as a calibrant by Gauy's method. The magnetic susceptibility (μ_{eff}) values of 1.70-1.74 B.M. observed for complexes **1-3** at room temperature correspond to the spin only value (S = 1/2) indicative of their mononuclear and paramagnetic nature and +4 oxidation state of vanadium atom.

3.8 Reactions with nitrogen bases

The reactions of **1** with equimolar amounts of 2-cyanopyridine and 4-aminobenzonitrile in methanol afforded the formation of dark brown 1:1 coordination compounds (**2** and **3**) in agreement with the elemental analysis and molar conductance measurement.The formation of the compounds has been confirmed from comparison of their FTIR spectra with **1** and free nitrogen bases. The coordination sensitive bands of 2-cyanopyridine due to υ(CN), υ(C=C), and υ(C=N) modes found to occurat 2240 cm^{-1}, 1600-1570 cm^{-1} and 1460-1430 cm^{-1} regions respectively. The υ(CN) mode appeared at 2240 cm^{-1} in 2-CNpy is known to shift to higher wave number when the free pair of electrons on the nitrogen of nitrile is involved in coordination resulting the increase in carbon-nitrogen bond order. On the other hand, the involvement of the cyano group through its triple bond or π-electrons results in decrease of υ(CN) mode. The four principal bands due to υ(C⎓C and C⎓N) modes of 2-cyanopyridine are found to occur at 1595, 1570, 1461 and 1430 cm^{-1}. The bands due to ring breathing mode of vibration occur at 985 and 1038 cm^{-1} [63]. The υ(C≡N) mode of 2-cyanopyridineis appeared at 2240 cm^{-1} in coordination compound $[VO(HL)_2.(C_6H_4N_2)]$ (**2**). No change in υ(C≡N) mode may be attributed to the non-participation of the cyano group in coordination. The bands due to υ(C-C) and υ(C-N) modes have been observed to move to higher wave numbers upon metal coordination. The coordination through the pyridine ring nitrogen only has thus been inferred establishing thereby the monodentate nature of the ligand. The absorption bands observed in 350-315 cm^{-1} region have been assigned to υ(N→V)

mode further substantiating the bonding of 2-cyanopyridine to vanadium atom through nitrogen. The peak at 935 cm^{-1} could be assigned to the υ(V=O) mode of vibration (Table S5).

The characteristic bands of free 4-aminobenzonitrile are found to appear at ~ 3360 cm^{-1}, ~ 3440 cm^{-1}, and ~ 2240 cm^{-1} against υ(NH) symmetric, υ(NH) asymmetric, and υ(CN) modes respectively. While coordination through nitrogen of the CN group is known to result in a shift of υ(CN) mode to higher wave numbers, bonding through nitrogen of $–NH_2$ group leads to a characteristic shift to lower wavenumbers. The IR spectra of coordination compounds of $[VO(HL)_2]$ with 4-aminobenzonitrile (**3**) have shown that the bands due to $υ_{asym}$(NH) and $υ_{sym}$(NH) vibrational mode have remained almost unaltered after coordination. It is observed that a significant shifting of 30-40 cm^{-1} in υ(CN) mode towards higher wave number has been occurred [64-66]. These observations suggest that nitrogen of amino ($-NH_2$) group is not involved in coordination with the metal while nitrile (CN) gets coordinated to the metal through its nitrogen. These observations are markedly in contrast with those found for coordination compounds of copper(II) halides with these ligands wherein bonding through nitrogen of $–NH_2$ had been proposed [67]. An explanation for the observations that coordination of 4-aminobenzonitrile has occurred through nitrogen of nitrile group and not amino group may be attributed to an inherent electron withdrawing property of nitrile group from the ring through resonance which results in the reduction of donor character of amino group in 4-aminobenzonitrile. The sharp and distinct bands observed in 338-325 cm^{-1} in **3** have been assigned to υ(N→V) mode [68-70]. The band due to υ(V=O) mode occurs at 1045 cm^{-1} in parent complex **1** have been found to shift to lower frequency and appeared at 925 cm^{-1} region in **3** (Table S6). This observation may be explained on the basis of donation of electronic from ligand N to vanadium (N→V) which increases the electron density on the metal d-orbitals and consequently reduces the $p_π → d_π$ donation from the oxygen atom to vanadium.

Based upon the physicochemical and IR spectral data, a hexacoordinate environment around vanadium depicting monodentate nature of 2-cyanopyridine bonding through pyridine ring nitrogen and that of 4-aminobenzonitrile through cyano group may tentatively be proposed.

3.9 Antibacterial activity

$VOSO_4·5H_2O$, potassium-4-nitrocinnamohydroxamate and complexes **1-3** were tested *in vitro* to assess the antibacterial activity against *Gram +ve* bacteria viz. *Staphylococcus epidermidis,* and

Staphylococcus aureus, Gram –ve bacteria Salmonella typhi, Escherichia coli, Salmonella paratyphi, and Klebsiellapneumoniae using MIC method (Figure 1).

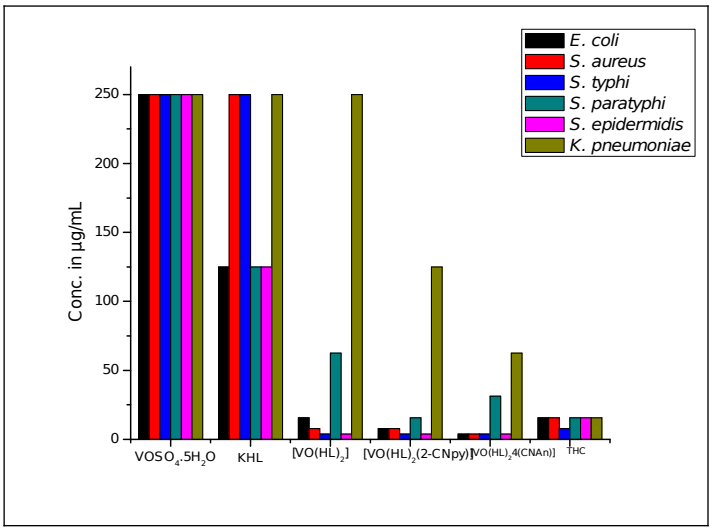

Figure 1. Comparative results for antibacterial activity of $VOSO_4 \cdot 5H_2O$, KHL, **1**, **2**, and **3**.

The results were compared with tetracycline hydrochloride (TCH) (a commercial antibiotic) as treated control which inhibited bacteria to 7.81-15.62 µg/mL range. The $VOSO_4 \cdot 5H_2O$ inhibited the growth of the test bacteria at 250 µg/mL. The ligands suppressed *S.epidermidis*, *E. coli* and *S. paratyphi* at 125 µg/mL and *S. aureus, S. typhi,* and *K. pneumonia* at 250 µg/mL level. Complex **1** showed good inhibitory effect against *S. typhi* and *S. epidermidis* at 3.9 µg/mL and *E. coli*, *S. aureus* and *S. paratyphi* at 15.62 µg/mL, 7.81 µg/mL, 63.5 µg/mL respectively. **1** has reactivity similar to standard drug for *E. coli* while have improved activity for *S. aureus* and less active for *S.paratyphi*. **2** showed the enhanced antibacterial activity against *E. coli, S. paratyphi* and *K. pneumoniae* over the complex **1**. Complex **3** inhibited *E.coli*, *S. aureus*, *S. paratyphiat* and *K. pneumoniae* at improved MIC relative to parent complex. The compounds under the study inhibited the growth of all *Gram +ve* and *Gram -ve* bacteria, showing an overall good activity which indicates their possible exploitation as future drugs. The inhibitory effect of ligand, $VOSO_4 \cdot 5H_2O$ and synthesized complexes is given in Table 1.

Table 1. The antibacterial activity of KHL, $VOSO_4 \cdot 5H_2O$, 1, 2, and 3.

Ligand/complex	*Bacteria*					
	E.coli	*S.aureus*	*S.typhi*	*S.paratyphi*	*S.epidermidis*	*K.pneumonae*
$VOSO_4 \cdot 5H_2O$	250	250	250	250	250	250
KHL	125	250	250	125	125	250
$[VO(HL)_2]$ (**1**)	15.62	7.81	3.9	62.5	3.9	250

$[VO(HL)_2(2\text{-}CNpy)]$ (**2**)	7.81	7.81	3.9	15.62	3.9	125
$[VO(HL)_2(4\text{-}CNAn)]$ (**3**)	3.9	3.9	3.9	31.25	3.9	62.5
Tetracyclinehydrochloride (Standard drug)	15.62	15.62	7.81	15.62	15.62	15.62

3.10 Antifungal activity

The ligand KHL, $VOSO_4 \cdot 5H_2O$ and complexes **1-3** were screened *in vitro* for their antifungal activity on selected fungi, viz. *B. fulva, A. niger*, and *M. circenelloids* by MIC method (Table 2). The results were compared with fluconazole (a standard antifungal drug) as treated control which inhibited these fungi at 3.9µg/mL. The $VOSO_4 \cdot 5H_2O$ inhibited the growth of selected fungi *M.circenelloids* at 15.62 µg/mL and *A. niger* and *B. fulva* at 62.5 µg /mL. The potassium-4-nitrocinnamohydroxamate inhibited fungi *A. niger* and *B. fulva* at 250 µg /mL and *M. circenelloides* at 62.5µg /mL. Complex **1** inhibited the growth of fungi *A. niger and M. circinelloides* at 7.81 µg/mL and that of *B. fulva* at 15.62 µg/mL showing better activity (Figure 2). **2** showed increased inhibitory effect against *A. niger* and *B. fulva* than complex **1** while complex **3** showed enhanced antifungal activity against all the test fungi relative to parent complex. The enhanced antimicrobial activity can be described on the basis of metal-ligand complexation by which the positive charge of the metal center is partially reduced due to sharing of electrons by the N-bases. This favors the permeation of the complex through the lipid bilayer of cell membrane [71]. Therefore, the synthesized complexes particularly **2** and **3** have promising antimicrobial activity in comparison to vanadyl sulphate and hydroxamate ligand.

Table 2. The antifungal activity of KHL, $VOSO_4 \cdot 5H_2O$ and the synthesized complexes.

Ligand/complex	*A.niger*	*B.fulva*	*M. circinelloids*
$VOSO_4 \cdot 5H_2O$	62.5	62.5	15.62
KHL	250	250	62.5
$[VO(HL)_2]$ (**1**)	7.81	15.62	7.81
$[VO(HL)_2(2\text{-}CNpy)]$ (**2**)	3.9	7.81	7.81
$[VO(HL)_2(4\text{-}CNAn)]$ (**3**)	3.9	7.81	3.9

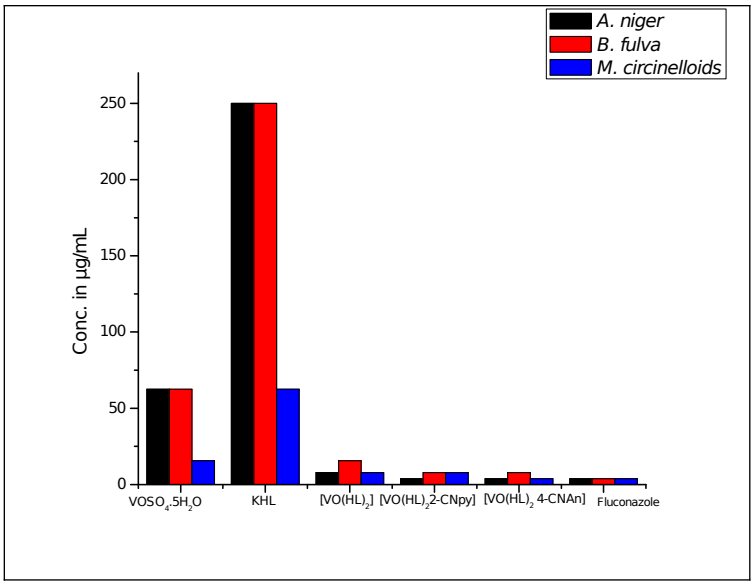

Figure 2. Comparative results for antifungal activity of $VOSO_4 \cdot 5H_2O$, KHL, **1**, **2**, and **3**.

3.11 *In Vitro* Cytotoxicity Assay

The cytotoxic assay of $VOSO_4 \cdot 5H_2O$, potassium 4-nitrocinnamohydroxamate and complexes **1-3** was carried out at several concentrations by colorimetric microculture MTT assay. Complex **1** exhibited appreciable inhibition of 9.5% at 0.25 mM, 13% at 0.5 mM and 16.5 % at 1mM concentration. Complex **2** and **3** showed inhibition of 79.09 % and 80.01 % at 0.25 mM concentration respectively (Table 3). The graphical representation of cell inhibition by the ligand and complexes is shown in Figure S7. It is of interest to note that with increasing concentration of the complexes **1-3,** cytotoxicity gets significantly enhanced in complexes **2** and **3.** Therefore, the coordination of 2-CNpy and 4-CNAn nitrogen bases has marked cytotoxic effect.

Table 3. Inhibition (%) of oxovanadium(IV) complexes against Hep2C cell line in µg/mL.

Test Compound	Dose concentration								
	Control	0.25mM	0.50mM	1mM	2mM	4mM	8mM	20mM	28mM
$VOSO_4 \cdot 5H_2O$	100	35.0	44.5	54.8	60	65	65	70	70
KHL	100	20.0	27.6	22.6	69.2	71.4	74.2	75.1	78.9
$[VO(HL)_2]$ (**1**)	100	9.5	13.0	16.5	44.1	45.0	48.8	49.8	57.3
$[VO(HL)_2$(2-CNPy)] (**2**)	100	79.09	82.2	84.0	87.4	90.02	91.6	94.03	95.1
$[VO(HL)_2$(4-CNAn)](**3**)	100	80.01	83.4	85.20	86.1	89.9	92.02	93.1	96.1

3.12 Theoretical study

3.12.1 Structure and binding energy

First, we have optimized the geometry of $VOSO_4 \cdot 5H_2O$ and the ligand, 4-nitrocinnamohydroxamate (HL^-) using BP86/DEF method. Using their optimized geometry, the geometry of **1** (cis), **1** (trans), **2**, and **3** are optimized with all real frequency values and their molecular structures are shown in Figure 3. The hydroxamate contains two functional groups viz., anionic N-oxo ($-NHO^-$) and neutral carbonyl (-CO), any one or both of which may be involved in bonding with V-atom. Important bond lengths of HL^- and the complexes are listed in Table 4.

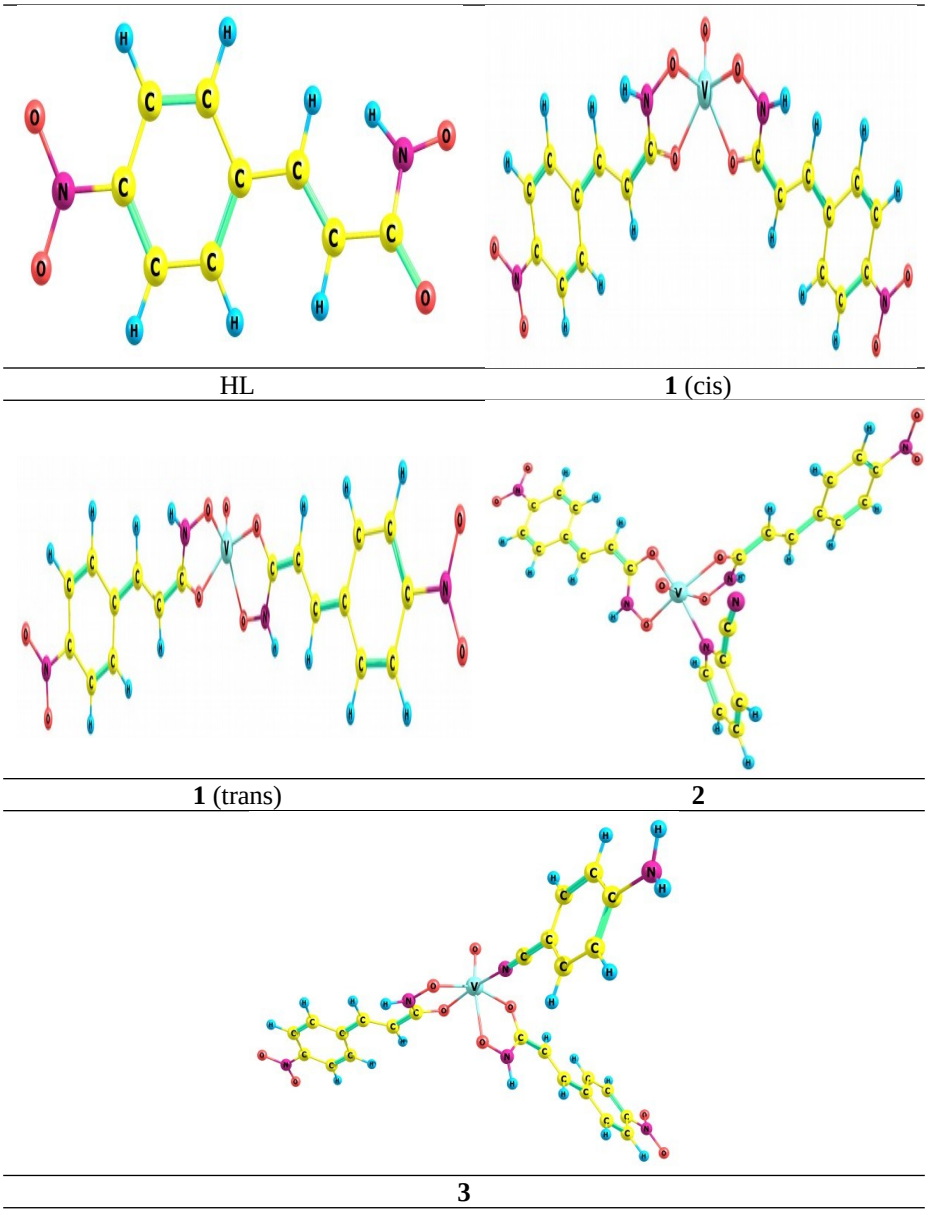

Figure 3. Optimized structures of HL, **1** (cis), **1** (trans), **2**, and **3** obtained using BP86/DEF method.

Both **1** (cis) and **1** (trans) structures got optimized with a distorted square pyramidal geometry around central vanadium atom. In these complexes, the vanadium atom is found to present 0.644 and 0.654 Å above the square plane formed by four O-atoms of the ligand. In cis complex, a mirror plane along the axial V=O bond and perpendicular to the horizontal square plane exactly divides the molecule in two parts. The average angle between V-O_{ax} and V-O_{eq} (O_{ax}-V-O_{eq}) is 108^o for cis complex and 109^o for trans complex respectively. In both the complexes the ligands are bonded as bidentate chelating ligand. The anionic O-atoms of the -NHO^- group of the ligand form stronger bonds (0.047 Å shorter) with V atom compared to the carbonyl oxygen atoms of the ligand. This is found to be opposite in case of complex **2** and **3**, where V-$O_{carbonyl}$ bonds are ~ 0.07 Å shorter for the both cases.

In **2** and **3**, central V atom is placed at the centre of a distorted octahedral geometry. Three O-atoms from two hydroxamate ligands and one N-atom of either 2-cyanopyridine or 4-aminobenzonitrile form equatorial square plane in **2** and **3** respectively. Vanadyl O-atom and O_{NO} of HL occupy the axial position of the octahedron. After the complexation of 2-cyanopyridine or 4-aminobenzonitrile with **1**, the V-$O_{vanadyl}$ bond length is increased slightly. This may be due to the strong binding of 2-cyanopyridine or 4-aminobenzonitrile with the V-atom, which weakens the axial orbital overlap. This also influences in the reduction of υ(V=O) mode of vibration in significant manner (vide supra, IR analysis). The V-$N_{pyridyl}$ in **2** and V-N_{CN} in **3** is calculated to be 2.159 Å and 2.071 Å respectively. The molecule where 2-cyanopyridine is attached through the cyano N-atom rather than the pyridyl N-atom with the V-atom has also been optimized. But, the latter complex is calculated to be 1.4 kJ/mol more stable than the former one in gas phase.

Table 4. Optimized structural parameters (in Å) of HL, **1** (cis), **1** (trans), **2**, and **3** calculated using BP86/DEF.

Ligand/complex	Selected Bond Distances					
	$R_{avg(C=O)}$	$R_{avg(N-O)}$	$R_{avg(V-O_{ax})}$	$R_{avg(V-O_{carbonyl})}$	$R_{avg(V-O_{N-oxo})}$	$R_{avg(V-N)}$
HL	1.244	1.285	-	-	-	-
1 (cis)	1.288	1.353	1.594	2.024	1.980	-
1 (trans)	1.286	1.355	1.594	2.026	1.977	-
2	1.283	1.344	1.599	2.034	2.104	2.159
3	1.284	1.339	1.600	2.039	2.109	2.071

Since binding energy calculation is a very important tool for analyzing the thermodynamic stability of the complexes, we have calculated the binding energy or complexation energy of the

studied complexes. The gas phase and solvent corrected complexation energies for **1** (cis), **1** (trans), **2**, and **3** have been calculated using BP86/def2-TZVP method in methanol-water (4:1 v/v) for **1** (cis and trans) and in methanol for **2**, and **3.** The corresponding free energies are given in the Table 5. The binding energy represents that all the synthesized complexes are thermodynamically stable. It can be observed that, the free energy of formation of **1** (cis) is slightly more negative (0.98 kcal/mol) as compared to **1** (trans) in solution. This indicates that, the formation probability of both the complexes in solution is nearly equal whereby these may coexist in the reaction medium.

Table 5. Free energy of formation and HOMO-LUMO energy gap of the complexes.

Complex	ΔG_{gas} (kcal/mol)	ΔG_{sol} (kcal/mol)	HOMO-LUMO (eV)
1 (cis)	81.74	-73.33	0.411
1 (trans)	82.79	-72.35	0.379
2	-0.91	16.98	0.217
3	-0.43	13.23	0.248

3.12.2 Global Reactivity Descriptors

The HOMO and LUMO energies of any compound are very important quantum chemical parameters and many physical and chemical properties can be calculated from these energies and the difference between them. Their energy difference is the direct indicative of the chemical reactivity or chemical inertness of any compound. This can be simply related to the ionization potential (IP) and electron affinity (EA) as: IP = - E_{HOMO} and EA = - E_{LUMO}. Chemical potential (μ), which is the amount of energy absorbed or released due to the change in particle number of the species in a chemical reaction, is also related to the HOMO and LUMO energies. The other parameters like hardness (η), softness (S), electronegativity (χ), and global electrophilicity index (ω) can also be calculated from HOMO-LUMO energy values. According to Koopman's theorem [ref] these parameters can be expressed by the following equations:

Chemical potential (μ)	= -(IP+EA)/2
Hardness (η)	= (IP-EA)/2
Softness (S)	= 1/2η
Electronegativity (χ)	= (IP+EA)/2
Global electrophilicity index (ω)	= $\mu^2/2\eta$

The magnitude of HOMO-LUMO energy difference of $VOSO_4 \cdot 5H_2O$ is 1.541 eV, which is reduced significantly after forming complex **1**. The value is less for trans complex than cis, which indicates the more reactivity of trans complex than cis. The value is further reduced in case of **2** and **3**, which provides direct support for more reactive nature of **2, 3** than **1**. This result is also in the same line as obtained from the experiment, as complexes **2** and **3** display higher microbial activity than **1**. The calculated value of the reactivity parameters of **1**, **2**, and **3** are presented in Table 6. The high negative chemical potential values of all the complexes signify the high stability of the complexes and suggest that the decomposition of the complexes into elements is unlikely. The small magnitude of chemical hardness and high values of chemical softness of the compounds reveal that the compounds are highly covalent in nature with minimum ionic character. It is interesting to note that, the hardness is still lesser for complexes **2** and **3** than **1** whereas softness trend is reverse. This clearly supports the relatively higher biological activity of **2** and **3** compared to **1** which may be due to higher penetration (higher lipophilicity) ability of **2** and **3** inside the individual cell (intracellular region) and easily react with the corresponding biological site. The high electrophilicity index values are characteristic of good nucleophile–electrophile combination in the complexes.

Table 6. The calculated reactivity parameters of **1**, **2**, and **3.**

	1 (cis)	**1** (trans)	**2**	**3**
Ionization potential (eV)	4.532	4.522	4.264	4.093
Electron affinity (eV)	4.121	4.143	4.047	3.845
Chemical hardness eV)	0.206	0.190	0.109	0.124
Chemical potential (eV)	-4.327	-4.333	-4.156	-3.969
Chemical softness (eV^{-1})	2.427	2.632	4.587	4.032
Global electrophilicityIndex (eV)	45.441	49.416	79.228	63.516
Electronegativity (eV)	4.327	4.333	4.156	3.969

3.12.3 Population analyses

In order to analyze the nature of bonding between the ligand and metal ion, the charges on metal ion as well as on the donor atoms of the ligands using natural population analysis (NPA) (Table S7) and Mulliken Population Analysis (MPA) (Table S8) have been calculated. A perusal of data has shown that, while the positive charge of V-atom in $VOSO_4 \cdot 5H_2O$ remains almost unaltered in **1 (**cis) and **1 (**trans), it is reduced by 0.15 (avg) and 0.26 (avg) in **2** and **3** as obtained from NPA and MPA respectively. This is indicative of higher charge transfer from ligand to V-atom in case of **2** and **3** than both **1** (cis) and **1**(trans) complexes. Moreover, the negative charge of vanadyl O-

atom is reduced in all complexes with respect to vanadium precursor, $VOSO_4 \cdot 5H_2O$ which indicates the lower charge transfer from ligand to V upon complexation as compared to anionic SO_4^{2-} to V in $VOSO_4 \cdot 5H_2O$ and ascribed more ionic character of $VOSO_4 \cdot 5H_2O$ relative to coordination complexes. From the negative charges on O-atoms of C=O and N-O, it can be inferred that, the charge of O_{CO} is reduced more than O_{NO} in the complexes relative to the free ligand according to NPA analysis. Albeit the reverse trend has been observed from the MPA analysis.

3.12.4 Density of states calculations

Total density of states (TDOS) and partial density of states (PDOS) and overall population density of states (OPDOS) of the synthesized complexes (**1**-**3**) have been calculated to find out the contribution of atomic orbitals to the molecular orbital. The DOS plots exhibit the population analysis per orbital and PDOS plots demonstrate percentage contribution of a particular group to each molecular orbital of complex. OPDOS diagram is helpful to find out the bonding and antibonding type of interaction between two groups. A positive value of OPDOS signifies bonding type interaction, while a negative value indicates an antibonding interaction and zero value is indicative of non-bonding interactions. The DOS, PDOS and OPDOS plots for ligand HL and complexes **1**, **2**, and **3** are presented in (Figure 4). From the PDOS plots of **1**, **2**, and **3** it can be inferred that, while HL orbitals have highest contribution towards bonding in complex **1,** HL and 2-cyanopyridine (or 4-aminobenzonitrile) orbitals have almost equal contribution in complex **2** and **3** respectively. The positive value of OPDOS of HL and V-metal atom in the bonding region in **1**, **2**, and **3** indicates that, ligand and V-metal have bonding interactions which stabilizes each complex.

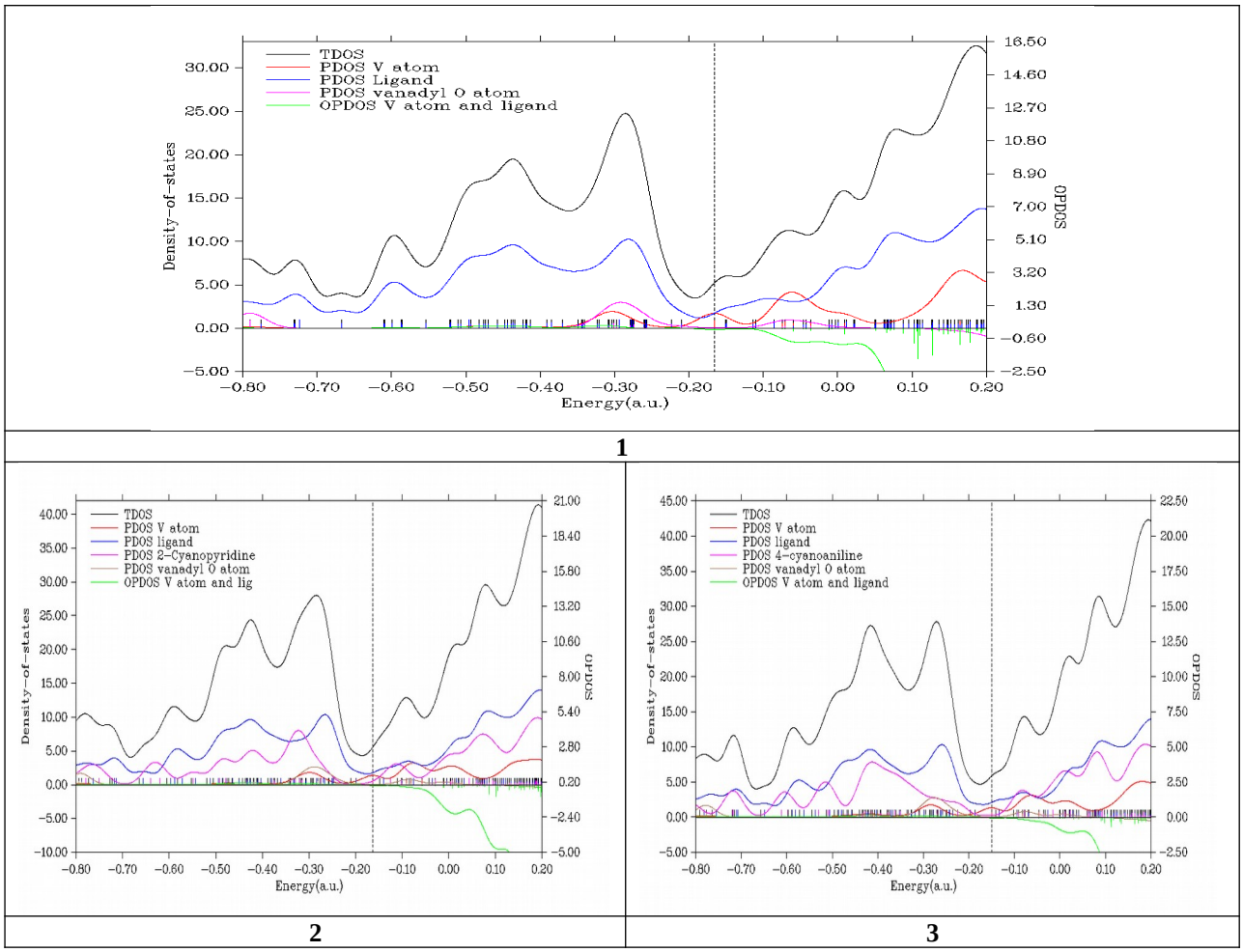

Figure 4. The DOS, PDOS and OPDOS plots of **1**, **2**, and **3.**

3.12.5 TD-DFT analysis

We have theoretically determined the nature of transition, their oscillation strength and percentage contribution for the electronic transitions of HL, **1**(cis), and **1** (trans) complexes in methanol. Table 7 shows the details of the results for HL, **1**(cis), and **1** (trans) complexes in methanol. A fair agreement is observed between the experimental and calculated spectra of the ligand and the complex except few additional peaks originated in the theoretical spectra (Figure S8) which probably quenched in solution. Figure 5 shows few frontier molecular orbitals, related to the transitions which are characteristics of high oscillation strength ($f > 0.01$) and lower energy (isosurface value = 0.05). It can be seen that, whereas HOMO-2 of the ligand are mainly localized on aromatic phenyl unit with π character, HOMO belongs to the non-bonding orbitals of CO and NO group O-atoms. The LUMO+2 and LUMO+3 of the ligand can be denoted as π anti-bonding orbitals. According to the theoretical calculations, two π-π* transitions (HOMO-2

to LUMO+2) at 245 and (HOMO-8 to LUMO) at 267 nm respectively and an n-π* transition (HOMO to LUMO+3) at 297 nm are observed. The stronger peaks at 246 and 290 nm and the weaker peak at 258 nm in the experimentally observed spectrum are in close agreement with the theoretically predicated transitions. Whereas, the HOMO-4 of **1** (cis) is localized on the overall ligand moiety, the HOMO-1 and HOMO-2 is mainly concentrated to the chelate rings of the ligands with π-character. Based on calculations, four major peaks are identified at 371, 428, 547, and 683 nm respectively with different oscillation strengths which are basically intra-ligand transitions with slight contribution of LMCT transition (O-p orbital (lone pair) to V-3d orbital). The experimentally observed peaks at 386, 422, 580, and 710 nm are in good agreement with the theoretically predicated transitions. The LUMO+1 and LUMO+3 are mainly composed of d-orbitals (d_{yz}: 12.22 % for LUMO+1 and d_{yz}: 49.11 %, d_{xy}: 3.53 % for LUMO+3) of the vanadium metal center which indicates the involvement of the metal orbitals in LMCT transitions. Similarly the frontier molecular orbitals are also calculated for the trans complex for comparison purpose. The HOMO-4, HOMO-2, and HOMO-1 are found to be akin to the cis complex. Here the identified four major peaks at 372, 420, 553, and 676 nm respectively with different oscillation strengths are also intra-ligand type of transitions with little contribution of LMCT transition.

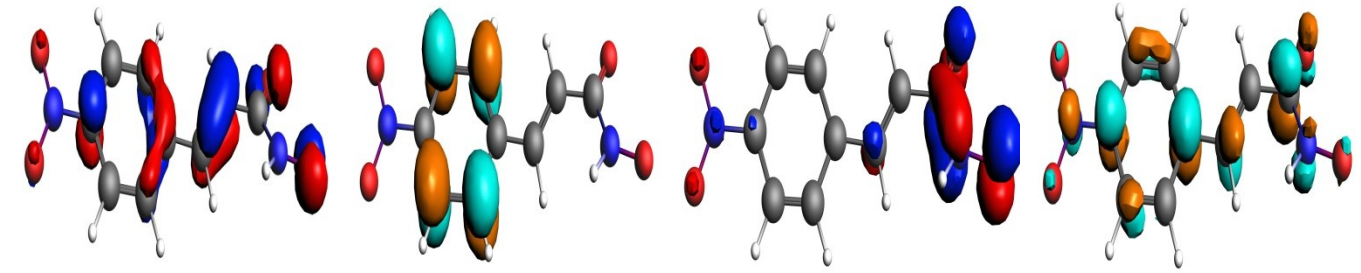

HOMO-2 LUMO+2 HOMO LUMO+3

HL

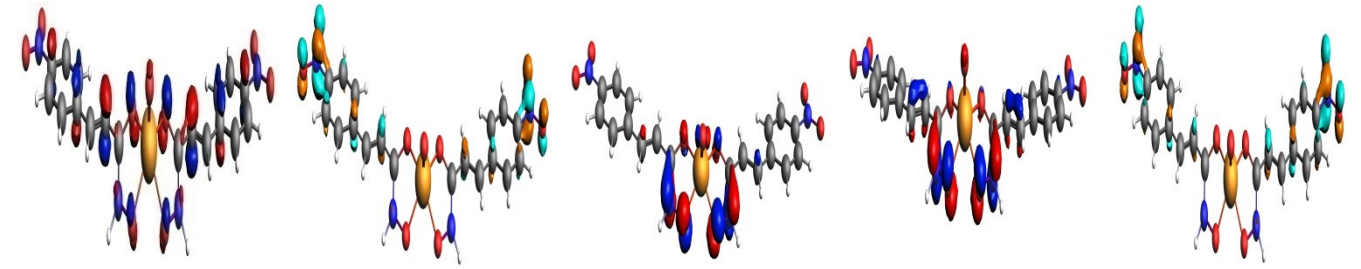

HOMO-4 LUMO HOMO-1 HOMO-2 SOMO

1 (cis)

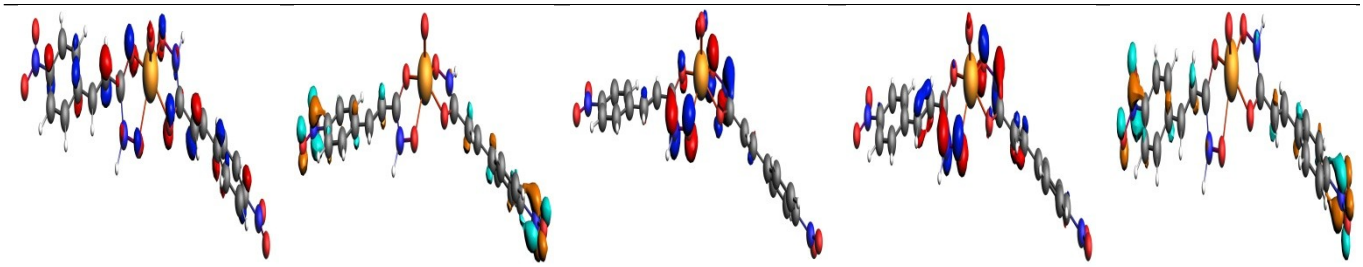

1 (trans)

Figure 5. Frontier molecular orbitals related to the transitions with high oscillation strength (f > 0.01) (Color code: brown: V, red: O, blue: N, Grey: C, White: H). Molecular orbitals are obtained at BP86/TZ2P computational level.

Table 7. Details of important UV-Vis transitions of HL, **1**(cis), and **1** (trans) in CH_3OH calculated from TD-DFT.

Ligand/complex	Calculated transition/nm	Composition	Oscillation strength (f)	Assignment
HL	245	H-2 to L+2(25.0%) H-5 toL+1(23.7%) H-3to L+2(22.1%)	0.194	π-π*
	267	H-8 to L (25.5%) H-2 toL+1(14.1%) H-5 to L+1(13.1%)	0.055	π-π*
	297	H toL+3(52.7%) H-3 to L+1 (23.8%) H-2 toL+1 (11.5%)	0.171	n-π*
1(cis)	371	H-4 to L (22.0%) H-3 to S (14.1%) H-1 to L+3 (14.0%) H-4 to L+1 (13.5%)	0.794	Intraligand Intraligand n(N,O) to d-orbital of V Intraligand
	428	H-1 to L (54.3%) H-1 to L+1 (23.2%)	0.115	Intraligand n(N,O) to d-orbital of V
	547	H-2to L(50.1%) H-2 to L+1(30.6%)	0.307	Intraligand Intraligand
	683	H-1 to S (58.1%) H-1 to L (29.7%)	0.107	Intraligand Intraligand
1 (trans)	372	H-4 to S(19.5%) H-3 to L(16.6%) H-4 to L (12.0%) H-3 toL+1(10.4%)	1.315	Intraligand Intraligand Intraligand Intraligand
	420	H-1 toL+1(40.0%) H-1 to L+2(25.6%)	0.027	n(N,O) to d-orbital of V Intraligand
	553	H-2 to S (47.2%) H-2 to L (28.6%)	0.450	Intraligand Intraligand
	676	H-1 to L (50.0%)	0.059	Intraligand

	H-1 to L+1 (26.4%)	Intraligand

4. Conclusion

The new bis(4-nitrocinnamohydroxamato) oxidovanadium(IV) complex has been synthesized and characterized by various physicochemical and spectroscopic techniques. The bidentate chelating bonding of the hydroxamate ligand through carbonyl (C=O) oxygen and hydroxylamine (-NHO) oxygen atom has been inferred. A square-pyramidal geometry around vanadium was supported by DFT calculations. The thermal decomposition study of the complex has yielded VO_2 as the decomposition product. The 1:1 coordination compounds of **1** with 4-aminobenzonitrile and 2-cyanopyridine have also been synthesized and characterized. Bonding through pyridine ring nitrogen with 2-CNpy in complex **2** and through N-atom of CN of 4-CNAn in **3** with vanadium has been inferred. The complexes **1**-**3** have exhibited promising biological activity against test pathogenic fungi and bacteria and *in vitro* cytotoxic activities towards Hep2C cell line. The coordination of nitrogen bases has played a pivotal role in cytotoxic activity in **2** and **3** being more active than the parent complex. DFT analysis has demonstrated by more reactive and covalent nature of **2** and **3** than **1** which results in easy penetration through the cell membrane. TD-DFT calculated electronic transitions found to support the experimental electronic spectra fairly.

Acknowledgements

Sonika Sharma is thankful to CSIR, New Delhi, for providing financial assistance in the form of a Junior Research fellowship. The authors thank the Department of Science & Technology (DST) Government of India, New Delhi, for providing financial assistance for FT-IR and UV-VIS facility to the Department under FIST program. The authors thank the Sophisticated Analytical Instrument Facility, Panjab University, Chandigarh, for elemental analysis and mass spectra, IIT, Roorkee for TGA-DTA and IIT Bombay ESR studies, Department of Physics of H.P.U. Shimla for magnetic moment measurements and Department of Biotechnology H.P.U. Shimla for carrying out biological studies. Sincere thanks are due to Computer Centre, BARC for providing ANUPAM parallel computational facility. D. Das would like to acknowledge Dr. C. P. Kaushik, Shri Anand Gangadharan and Dr. A. S. Pente for their continuous support and encouragement for the work.

References:

1. D. Wen, J. Zhou, H. H. Zou, J. Coord. Chem. 72 (2019) 1064-1074.
2. J.G. Vijayan, Biomed. J. Sci. Tech. Res. 3 (2018) 3264-3266.
3. I. Soghli, A.D. Khalaji, G. Grivani, Inorg. Chem. Res. 5 (2021), 163-172.
4. K. S. Prasad, S. U. Ramachandrappa, Curr. Bioact. Comp. 16 (2020) 201-209.
5. K. Gruzewska, A. Michno, T. Pawelczyk, H. Bielarczyk, J. Physiol. Pharmacol. 65 (2014) 603-611.
6. A. K. Srivastava, Mol. Cell Biochem. 206 (2000)177-182.
7. M. Fernandez, L. Becco, I. Correia, J. Benitez, O. E. Piro, G. A. Echeverria, A. Medeiros, M. Comini, M. L. Lavaggi, M. González, H. Cerecetto, V. Moreno, J. C. Pessoa, B. Garat, D. Gambino, J. Inorg. Biochem. 127 (2013) 150-160.
8. S. A. Zabin, M. Abdelbaset, Euro. J. Chem. 7 (2016) 322-328.
9. A. Sheela, R. Vijayaraghavan, J. Coord. Chem. 64 (2011) 511-524.
10. E. J. Baran, J. Inorg. Biochem. 80 (2000) 1-10.
11. A. Mei Li, J. Coord. Chem. 67 (2014) 2076-2085.
12. D. Rehder, Fut. Med. Chem. 14 (2012) 1823-1837.
13. I. F. Persoon, M. A. Hoogenkamp, A. Bury, P. R. Wesselink, A. F. Hartog, R. Wever, W. Crielaard, J. Endodontics 39 (2013)1035-1038.
14. S. Shahzadi, S. Ali, M. Parvez, A. Badshah, E. Ahmed, A. Malik, Russ. J. Inorg. Chem. 52 (2007) 386-393.
15. N. Sharma, M. Kumari, V. Kumar, S.C. Chaudhry, S.S. Kanwar, J. Coord. Chem. 63 (2010) 176-184.
16. A. I. Sidorov, O. P. Vinogradova, T. A. Khrushcheva, I. E. Obyknovennaya, G. N. Ermolaeva, V. B. Shilov, J. Opt. Tech. 75 (2008) 33-37.
17. S. C. Davies, D. L. Hughes, Z. Janas, L. B. Jerzykiewicz, R. L. Richards, J. R. Sanders, J. E. Silverston, P. Sobota, Inorg. Chem. 39 (2000) 3485-3498.
18. A. C. Niedwieski, P. B. Hitchcock, J. D. Da Motta Neto, F. Wypych, G. J. Leigh, F. S. Nunes, J. Braz. Chem. Soc. 14 (2003) 750-758.
19. A. S. Gaballa, S. M. Teleb, M. S. Asker, E. Yalcin, Z. Seferoglu, J. Coord. Chem. 64 (2011) 4225-4243.
20. R. E. Tapscott, R. L. Belford , I. C. Paul, Inorg. Chem. 7 (1968) 356-364.
21. F. A. El-Saied, T. A. Salem, S. A. Aly, M. M. E. Shakdofa, Pharm. Chem. J. 51 (2017) 833-842.
22. P. de A. Machado, V. Z. Mota, A. C. de L. Cavalli, G. S. G. Carvalho, A. D. Da Silva, J. Gameiro, A. Cuin, E. S. Coimbra, Acta Tropica. 148 (2015) 120-127.
23. D. Crans, M. M. Tahir, M. Johnson, P. C. Wilkins, Inorg. Chim. Acta. 356 (2003) 365-378.
24. G. Scalese, M. F. Mosquillo, S. Rostan, J. Castiglioni, I. Alhz, L. Perez, I. Correia, F. Marques, J. C. Pessoa, D. Gambino, J. Inorg. Biochem. 175 (2017) 154-166.
25. J. G. Vijyan, Biomed. J. Sci. Tech. Res. 3 (2018) 3264-3266.
26. M. Pisano, C. Arru, M. Serra, G. Galleri, D. Sanna, E. Garribba, G. Palmieri, C. Rozzo, Metallomics 11 (2019) 1687-1699.
27. A. D. Keramidas, S. M. Miller, O. P. Anderson, D. C. Crans, J. Am. Chem. Soc. 119 (1997) 8901-8915.
28. S. Hati, R. J. Batchelor, F. W. B. Einstein, A. S. Tracey, Inorg. Chem. 40 (2001) 6258-6265.
29. D. C. Crans, P. K. Shin, A. S. Tracey, Inorg. Chem. 27 (1988) 1797-1806.
30. M. J. A. Abualreish, M. A. Abdein, Adv. Chem. Ser. 10 (2014) 2118-2125.

31. B. Shireen, N. Khan, Samiullah, I. Ali, A. Akbar, A. -ur- Rehman, F. Behlil. Pure Appl. Biol. 9 (2020) 2199-2206.
32. S. P. Li, S. M. Hu, Trop. J. Pharm. Res. 19 (2020) 957-963.
33. C. Ning , Y. Bi, Y. He, W. Y. Huang, L. Liu, Y. Li, S. Zhang, X. Liu, N. Yu, Bioorg. Med. Chem. Lett. 23 (2013) 6432-6435.
34. T. Buxton , S. Takahashi , A.-M. E. Doh , J. B. -Ansah , E. O. Owusu, C. -Sa Kim, Pest. Manag. Sci. 76 (2020) 257-267.
35. P. De, M. Baltas, F. Belval, Curr. Med. Chem, 18 (2011) 1672-703.
36. E. Pontiki, D. H. Litina, K. Litinas, G. Geromichalos, Molecules 19 (2014) 9655-9674.
37. A. Tavares, R. O. Costa, Caroline S. B. Weber, T. Cazati, M. A. Ceschi, A. A. Vieira, A. A. Merlo, J. Braj. Chem. Soc. 32 (2021) 98-109.
38. N. Sharma, S. S. Kanwar, R. Gupta, L. Kumari, R. Sharma, Bull. Chem. Soc. Jpn. 85 (2012) 1310-1317.
39. N. Sharma, M. Kumari, V. Kumar, S. C. Chaudhry, J. Enzym. Inhib. Med. Chem. 708 (2010) 708-714.
40. V. K. Choudhary, A. K. Bhatt, D. Dash, N. Sharma, J. Comput. Chem. 40 (2019) 2354-2363.
41. V. K. Choudhary, A. K. Bhatt, D. Dash, N. Sharma**,** Appl. Organomet. Chem. 34 (2020) e5360.
42. V. K. Choudhary, A. Kumar, N. Sharma, Main Group Met. Chem. 41 (2018) 27-32.
43. V. K. Choudhary, A. K. Bhatt, N. Sharma, J. Coord. Chem. 72 (2019) 372–387.
44. V. K. Choudhary, S. Bhardwaj, A. K. Bhatt, N. Sharma, J. Comp. Methods Sci. Eng. 20 (2019) 157-166.
45. A. Kumar, M. Sharma, Bhanu Priya, V. K. Choudhary, N. Sharma, Proc. Natl. Acad. Sci., Ind, Sect. A Phys. Sci. 20 (2019) 157-166.
46. S. Kumari, N. Sharma, J. Coord. Chem. 72 (2019) 1-14**.**
47. Bhanu Priya, A. Kumar, N. Sharma, Aust. J. Chem. 73 (2020) 61-72.
48. V. K. Choudhary, N. Sharma, J. Coord. Chem. 73 (2020) 947-968.
49. C. R. Hauser, W. B. Renfrow. Benzohydroxamic acid. Organic Syntheses. Coll. Vol. II, Edi. A.H. Blatt and Jahn Wiley and Sons, New York, 67-68 (1967).
50. T. J. Mackie, J. E. McCartney, J. G. Collee, *Practical Medical Microbiology:* 13th Edn, Churchill Livingstone, Edinburgh, 696 (1989).
51. D. Greenwood, R. Slack, J. Peutherer, Medical Microbiology A Guide to microbial infections: Pathogenesis, immunity, laboratory diagnosis and control, 15th ed. (1997).
52. (a) R. Ahlrichs, M. Bär, M. Häser, H. Horn, C. Kölmel, Chem. Phys. Lett. 162 (1989) 165-169 (b) TURBOMOLE V6.6 2014, a Development of University of Karlsruhe and Forschungszentrum Karlsruhe GmbH, 1989−2007, TURBOMOLE GmbH, since 2007, available from http://www.turbomole.com.
53. G. teVelde, F. M. Bickelhaupt, E. J. Baerends, C. Fonseca Guerra, S. J. A. van Gisbergen, J. G. Snijders, T. Ziegler, J. Comput. Chem. 22 (2001) 931-967.
54. A. Klamt, G. Schüürmann, J. Chem. Soc., Perkin Trans. 2 (1993) 799–805.
55. Tian Lu, Feiwu Chen, J. Comput. Chem. 33 (2012) 580-592.
56. A. K. Yadav, H. S. Yadav, S. Singh, U. S. Yadav, D. P. Rao, J. Chem. 2013 (2012) 1-5.
57. M. Haratake, M. Fukunaga, M.Ono, M. Nakayama, J. Biol. Inorg. Chem. 10 (2005) 250-258.
58. L. R. Hassan, H. Bahron, K. Ramasamy, A. M. Tajuddin, MJAS. 23 (2019) 263-273.
59. A. Eiman T, A. Othman, T. Shakir F, Res. J. Chem. Environ. 23 (2019) 1-13.

60. M. Saif, H.F. El-shafiy, M.F. Eid, A.I. Nabeel, R. Fouad, J. Mol. Structure, 1118(2016)1–42. 10.1016/j.molstruc.2016.03.060
61. E. Wenda, J. Therm. Anal. Calorim 20 (1981) 153-167.
62. I. L. Botto, M. B. Vassallo, E. J. Baran, G. Minelli, Mater. Chem. Phys. 50 (1997) 267-270.
63. A. Mishra, K. Mishra, U. C. Agarwal, Polyhedron 9 (1990) 863-874.
64. M. F. Farona, N. J. Bremer, J. Amer. Chem. Soc. 88 (1966) 3735-3737.
65. P. C. Ford, R. E. Clarke, J. Chem. Soc., Chem. Commun. 2 (1968) 1109-1110.
66. N. Sharma, A. K. Sood, S. S. Bhatt, S. C. Chaudhry, Polyhedron 16 (1997) 4055-4060.
67. I. S. Ahuja, S. Tripathi, Asia. J. Chem. 2 (1990) 229-238.
68. I. S. Ahuja, C. L. Yadava, S. Tripathi, Trans. Met. Chem. 13 (1988) 140-142.
69. X. Yang, K. Wang, J. Lu, D.C. Crans, Coord. Chem. Rev. 237 (2003) 103-111.
70. L. C. Yu, Z. L. Tang, P. G. Yi, S. L. Liu, X. Li, J. Coord. Chem. 62 (2009) 903-910.
71. D.C. Crans, J.J. Smee, E. Gaidamauskas, L. Yang, Chem. Rev.104(2004)849-902.